DOI: 10.13009/EUCASS2017-349

Performance Comparison between Extruded and Printed Ceramic Monoliths for Catalysts

Robert-Jan Koopmans, Sebastian Schuh, Tobias Bartok
FOTEC Forschungs- und Technologietransfer GmbH, Viktor Kaplan-Straße 2, 2700 Wiener Neustadt, Austria

Yann Batonneau, Corentin Maleix, Romain Beauchet
CNRS UMR 7285, IC2MP, University of Poitiers, Bât. B27, 4 rue Michel Brunet, TSA 51106, 86073 Poitiers cedex 9, France

Martin Schwentenwein, Manfred Spitzbart
Lithoz GmbH, Mollardgasse 85a/2/64-69, 1060 Wien, Austria

Carsten Scharlemann
Fachhochschule Wiener Neustadt GmbH, Johannes Gutenberg-Straße 3, 2700 Wiener Neustadt, Austria

Abstract

This paper presents the first results of monopropellant decomposition tests obtained from monolithic ceramic catalysts produced by means of additive layer manufacturing techniques and using ceramic precursors. The purpose is to compare the performance of printed monoliths with traditionally manufactured catalysts with respect to decomposition of highly concentrated hydrogen peroxide. Small holes with a pitch larger than 0 are generally difficult to manufacture. Holes with a diameter of 1.25 mm are difficult to manufacture when the pitch is larger than 2. Decomposition tests revealed that the manufacturing process does not influence the transient pressure performance but is noticeable in the transient temperature performance. However, the influence is only present during part of the transient phase. For optimum transient performance the surface area-to-volume ratio should be maximised.

1. Introduction

Monopropellant propulsion systems mostly rely on the rapid decomposition of a propellant on a catalyst. The net effect of the decomposition process is a significant rise in temperature of the products. Typical temperatures encountered in the reaction chamber range from about 945 °C for 98 wt. % hydrogen peroxide [1] to about 2200 °C for ionic propellants such as HAN (hydroxylammonium nitrate) or ADN (ammonium dinitramide) based propellants [2].
Over the past two decades, catalysts for high test peroxide (HTP), ADN and HAN propellant blends have received a lot of attention due to an increased interest in alternatives to hydrazine [3]–[6]. A particular difficulty with catalysts for ionic liquids is that a certain amount of preheating is required to initiate the decomposition process [7], [8]. This has system disadvantages such as necessary heating power (typically ~10 W for a 10 N thruster) and, in particular, the required time for pre-heating (typically 30 min). Although preheating of catalysts is common for hydrazine thrusters, the required level of preheating is generally less compared to catalysts for ionic liquids. Furthermore, hydrazine catalysts can be operated in cold conditions if necessary albeit shortening the catalyst lifetime, whereas decomposition of ionic liquids would not take place on a cold catalyst.
Typical requirements for catalysts are that the decomposition reaction is fast, that they operate over extended periods of time and that the pressure drop over the catalyst is minimal. Current state of the art catalysts are of the particulate type. Here the catalyst consists of particles with a predefined range of sizes and sometimes predefined shape. The particles themselves are not catalytic; they get their catalytic properties from an active phase with which the particles are impregnated. The most well-known catalyst of the particular type is the S405 catalyst, formerly Shell 405, used in hydrazine thrusters since the 60's [9]. Disadvantages of this type of catalyst are the high pressure drop over the bed and the tendency of attrition due to abrasion [10]. Current catalysts for HAN- and ADN-based propellants rely on the heritage from hydrazine thrusters and are thus of the particulate type.
The H2020 funded RHEFORM project aims at further developing the ADN technology in order to provide an alternative to hydrazine for a much wider field of space missions [11]. One of the goals is to develop catalysts that allow a lower amount of preheating. To develop such a catalyst several aspects are investigated, such as the choice of active phase, washcoat procedure, monolith material and shape. The latter refers to the internal and external shape of

DOI: 10.13009/EUCASS2017-349

the catalyst. Traditionally, monoliths are manufactured by pushing a ceramic paste through an extrusion die. The catalyst designer of such monoliths has the possibility to set the shape and size of the channels as well as the length of the monolith. However, the resulting monolith always has straight channels. As such, the design degrees of freedom is limited to two dimensions only.
Recently, a technique was developed by Lithoz GmbH to print ceramic structures [12]. Contrary to manufacturing by extrusion, printing makes monoliths with complex 3D internal structures possible. Within the RHEFORM project the first steps are taken to further develop catalysts based on additive layer manufacturing.
This paper presents the results of a series of tests with such monoliths performed as part of the RHEFORM project. The first set of tests was designed to identify manufacturing limitations and is described in section 2. The second set of tests consisted of decomposition tests to investigate the steady state and transient performance. The tests were performed with 87.5 wt. % HTP, but are believed to be a good representation for other propellants relying on decomposition. Section 3 describes the test objective and setup. The test procedure is explained in section 4. The results are presented in section 5 and further discussed in section 6.

2. Design limitations

As a first step, it was investigated what the manufacturing limitations are. For this purpose, three monoliths were printed from MgO. Sample 1 contained holes with 4 different diameters: 0.5, 0.75, 1.0 and 1.25 mm. Sample 2 and 3 both consisted of equilateral triangular shaped channels with a wall thickness of 0.22 mm. A schematic of the two different structures is shown in Figure 1.

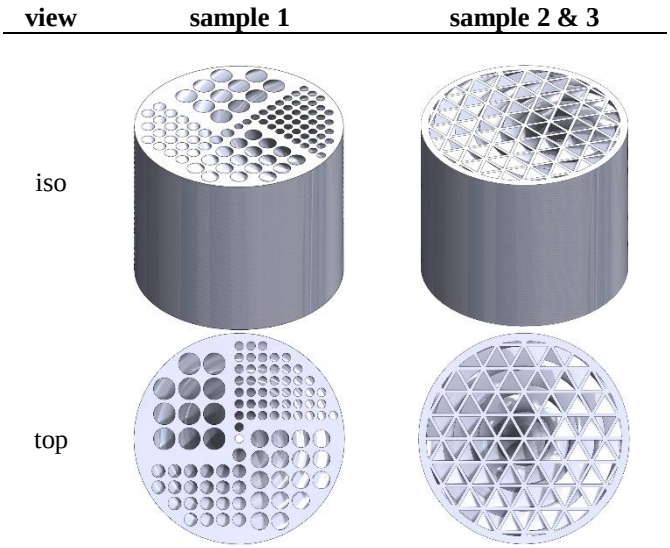

Figure 1: Iso- and top-view of the tested samples

All cylinders had a length of 10 mm. To investigate the 3D capabilities of the manufacturing procedure, the cylinder was twisted, i.e. the top plane was rotated relative to the bottom plane. Samples 1 and 3 were rotated 360 ° and sample 2 by 180 °. The samples were investigated by grinding them, taking pictures of the cross section and compare the different cross section pictures with each other.
The results for sample 1 are shown in Figure 2 and Figure 3. Both plots show the cross sectional areas of the holes relative to the top plane as a function of the pitch. Here, the pitch is defined as

$$pitch = \frac{2\pi r}{L} \tag{1}$$

Here, r is the distance of the centre of the channel to the centre of the monolith and L the required length of the monolith to rotate 360 ° once. The relative cross sectional areas at 4.43 and 9.11 mm from the top plane are shown in Figure 2 and Figure 3, respectively. Except for the holes with a diameter of 1.25 mm, no particular trend is discernible. One possible explanation for this is the way in which the green bodies are cleaned from the excess slurry. By immersing the green bodies in a solvent, removing excess slurry fully relies on diffusion. The smaller the hole diameter the higher the diffusion resistance and thus the lower the effective diffusion. The plots suggest that the critical diameter is between 1.0 and 1.25 mm. For holes with a diameter of 1.25 mm the pitch seems to play a role as well and becomes noticeable for a pitch of 2 and larger.

DOI: 10.13009/EUCASS2017-349

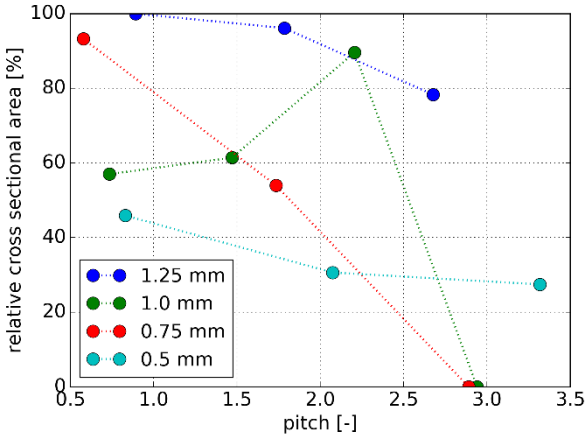

Figure 2: Relative cross sectional area at 4.43 mm for different hole diameters

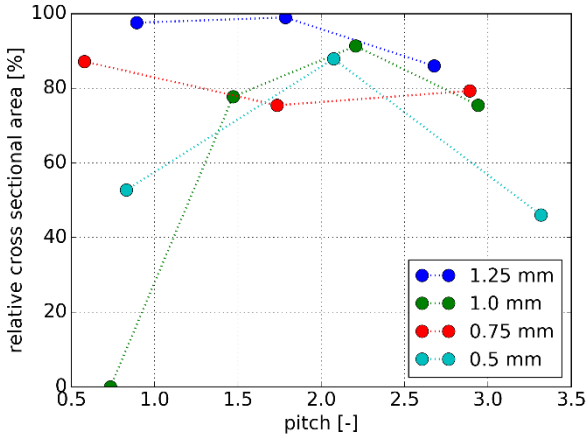

Figure 3: Relative cross sectional area at 9.11 mm for different hole diameters

The results for sample 2 and 3 are shown in Figure 4. The circular symbols refer to sample 2 and the triangles to sample 3. The plot shows that even for a small pitch, the cross section area is just above 80 %. This can partly be explained by the manufacturing process. Glare causes irradiation of the liquid adjacent to the intended structure, resulting in accidental curing of the liquid in areas that are supposed to remain available for fluid flow. This effect is especially noticeable at sharp corners. Subsequent dissolving excess slurry from these corners is also hindered by effective diffusion effects. The overall result is a smaller cross sectional area. For a pitch of up to about 1.5 the results are independent of the pitch. A pitch larger than 2.5 clearly affects the result, which was already concluded from Figure 2 and Figure 3.

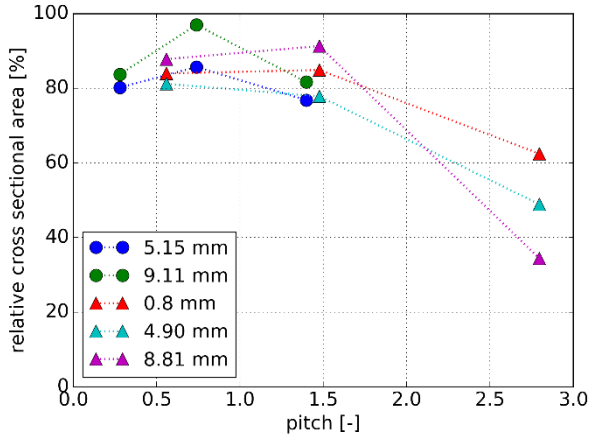

Figure 4: Relative cross section area for triangular channels at different positions from the top plane of the monolith

Note that the here presented structures were used to identify manufacturing limitations only. No regard was given to optimise the structures for transient response and pressure drop over the catalyst.

3. Test objective and setup

The goal of the test campaign was to determine how printed ceramic monoliths compare to traditionally manufactured ones. Extruded catalysts were extensively used by FOTEC in the past for the decomposition of 87.5 wt. % HTP [3], [13], [14]. For the current test campaign 87.5 wt. % HTP was used. It is believed that the results are equally relevant for other liquid propellants relying on decomposition over a catalyst, including HAN- and ADN-based propellants. HTP is considered as a good simuli propellant, being easier to implement because extensive preheating is not required and there is a large amount of experience with this fluid both at FOTEC and IC2MP.

The baseline for comparison was a monolith made from cordierite with 600 cpsi (channels per square inch) straight channels and a length of 10.1 mm. The monolith was washcoated with a dedicated sol to get an alumina-based porous layer and impregnated with Pt. This catalyst was compared to monoliths made from two different cordierite slurries. The difference between the two is the size of the ceramic particles in the solution. Two monoliths were printed from

DOI: 10.13009/EUCASS2017-349

each slurry. Subsequently, they were washcoated and impregnated in the same way as the extruded catalyst. These steps are described in more detail in [15].
The five catalysts were tested in a setup of which a CAD drawing is shown in Figure 5. A solenoid valve, hereafter referred to as FCV (flow control valve), controls the flow of HTP to the decomposition chamber. HTP is injected with a porous injector into the decomposition chamber where the catalyst is located. The injector head is fixed to the decomposition chamber by means of a flange and sealed by a copper ring. Downstream of the catalyst and upstream of the throat two K-type thermocouples are located: one in the centre of the chamber and one halfway between the centre and the decomposition chamber wall. An access port provides the access of the thermocouples to the interior of the decomposition chamber. The same port is also used for pressure measurements. In this way the dribble volume is minimised as much as possible. The disadvantage is that any pressure oscillations that may be present in the decomposition chamber will be attenuated and thus not be measured or measured to a limited extent only.

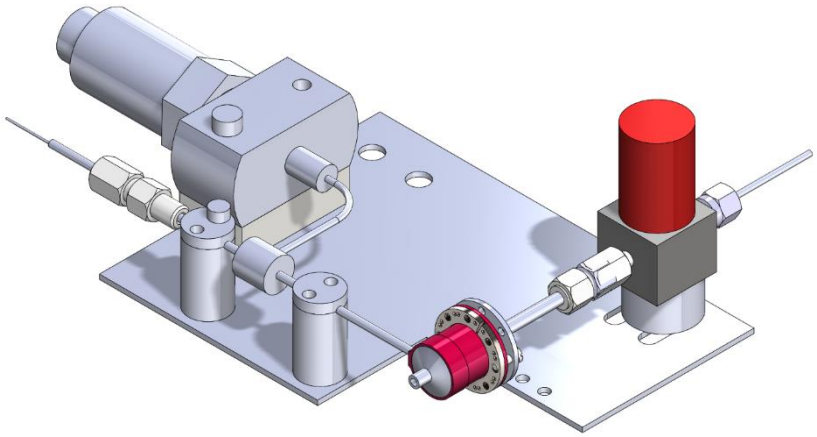

Figure 5: CAD drawing of the test setup

4. Procedure

Each catalyst in this comparison was fired four times. A typical test starts with the FCV closed. Temperature and pressure are recorded for 10 s. After 10 s the FCV is opened and remains open for 200 s. After 200 s the FCV is closed but the measurements continue for another 60 s. Finally, after the 270 s the test is finished. Throughout the whole tests all measurements are taken at a frequency of 100 Hz. The next test does not start before all measured temperatures are within two degrees of the ambient temperature. The whole test procedure is controlled by LabView.
The test results are used to investigate the steady state and transient performance of the temperature and the pressure. Steady state pressure and temperature are determined by taking the average of the values measured between 120 and 170 s into the test, i.e. the average over 50 s or 5000 measurement points. The transient performance is expressed in terms of the rise time and indicated as τ_P and τ_T for pressure and temperature, respectively. These performance indicators are explained with the help of Figure 6 and Figure 7.

DOI: 10.13009/EUCASS2017-349

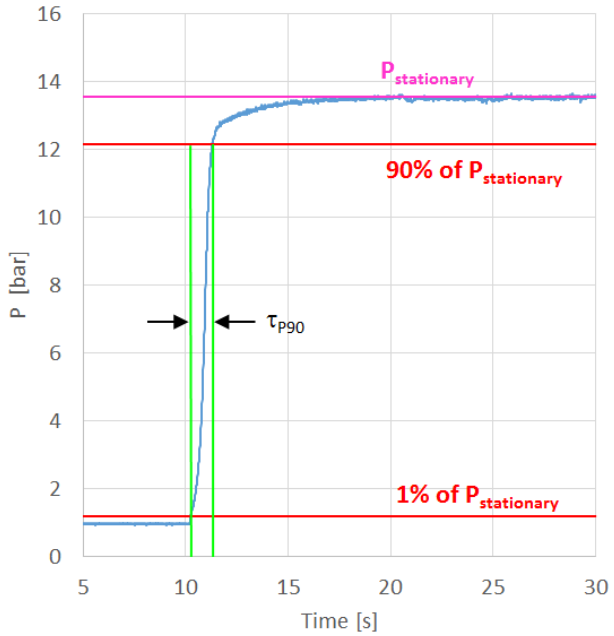

Figure 6: Definition of τ_P

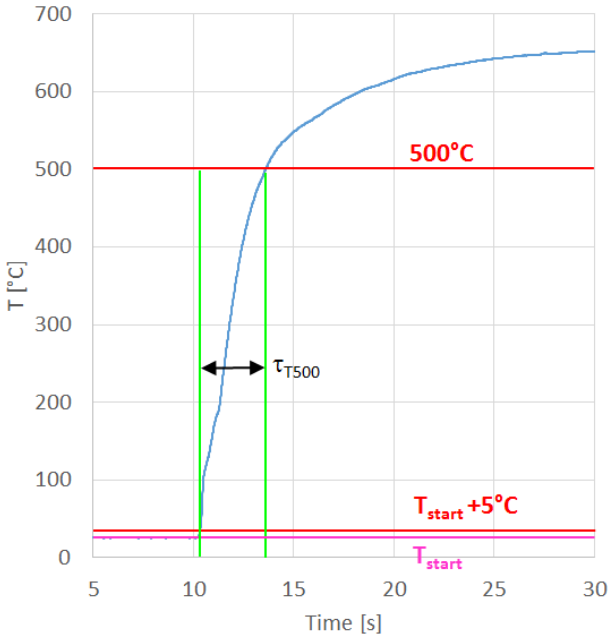

Figure 7: Definition of τ_T

For τ_P value the initial pressure level, $P_{initial}$, and the steady state pressure, P_{ss}, need to be measured. As is shown in Figure 6 the pressure rise is characterised by a steep increase to about 95 % of the total pressure increase followed by a gradual increase to its final steady state value.

The steep increase is due to the rapid increase in gas mass as a result of the reactions taking place in the chamber and the corresponding large increase in temperature. The gradual increase to the final steady state value is related to the time it takes for the structure to heat up and reach thermal equilibrium with its environment. The latter can be reduced by optimising the system design whereas the former is related to the reactivity of the system (catalyst effectiveness in case of decomposition and effectiveness of droplet breakup, mixing and evaporation in case of auto-ignition, thermal ignition and hypergolic reactions).

The pressure rise time is now defined as the time delay between the initial increase in pressure and the moment the pressure reaches a predefined fraction of the total pressure increase. The fraction is indicated with a number signifying the percentage of total pressure increase. So, τ_{P90} refers to the time elapsed between the initial pressure increase and the moment 90 % of the total pressure increase is reached. For practicality, the initial pressure increase is the moment at which the pressure increase has reached 1 % of the total pressure increase. If the total pressure increase is defined as $\Delta P_{ss} = P_{ss} - P_{initial}$, then $\tau_{P\alpha}$ is defined as

$$\tau_{P\alpha} = t\left(\frac{\alpha}{100}\,\Delta P_{ss}\right) - t\,(0.01\,\Delta P_{ss}) \tag{2}$$

where α indicates the percentage of total pressure increase. Figure 6 indicates the time delay for a value of α = 90, or τ_{P90}.

For the τ_T value the initial temperature needs to be measured and a threshold temperature needs to be defined. The initial temperature from which the time measurement starts is defined as the temperature at the start of the test plus 5 K. In this way the start time is unambiguously defined. The threshold value is a temperature of interest for the particular propellant. This can be, for instance, the temperature at which the liquid boils, at which thermal decomposition takes place or at which auto-ignition with a fuel occurs. The threshold temperature is indicated with a number in the subscript.

The temperature rise time is now defined as the time it takes for the temperature to climb from an initial increase of 5 K to α K, or

$$\tau_{T\alpha} = t(T = \alpha) - t(T = T_{initial} + 5\ \mathrm{K}) \tag{3}$$

Figure 7 shows the time delay to reach 500 °C, indicated as τ_{T500}. Note that for τ_T values the initial temperature needs to be specified. For a correct comparison the initial temperatures of tests and/or systems that are compared need to be the same or very similar. Here 'very similar' means that the deviation in comparison to the total temperature increase should be negligible.

DOI: 10.13009/EUCASS2017-349

5. Test results

Table 1 lists the loading characteristics, mass and dimensions of the tested catalysts. The monolith of catalyst GC299 was manufactured by means of extrusion; all others were printed. The designation C822 and C856 refer to the particular slurry that was used.
A large difference in monolith mass is apparent between the traditionally manufactured and the printed monolith, with the latter almost twice as heavy. The outer dimensions of all the monoliths are more or less the same. The explanation for the difference in mass should therefore be sought in the difference in wall thickness and porosity of the material. For all catalysts the relative amount of washcoat is very similar. The relative amount of active phase is similar for RM-C822-03 and RM-C856-06 compared to GC299. RM-C822-05 and RM-C856-04 have a higher amount of active phase.

Table 1: Loading characteristics and dimensions of tested catalysts

Catalyst name	mass monolith [g]	wt.% washcoat layer w.r.t. monolith	wt.% active phase w.r.t. washcoat layer	catalyst diameter [mm]	catalyst length [mm]
GC299	0.7123	14.1	26.3	11.78	10.08
RM-C822-03	1.3961	14.5	22.2	11.78	10.60
RM-C822-05	1.4705	13.1	59.0	11.86	10.54
RM-C856-04	1.2993	13.3	43.6	12.12	10.74
RM-C856-06	1.3053	14.0	27.7	12.16	10.71

Figure 8 and Figure 9 show the steady state temperature results for both slurries in comparison with GC299. The average temperatures are indicated by means of symbols. The error bars indicate the spread by means of twice the standard deviation. Also indicated in both figures is the adiabatic decomposition temperature of 87.5 wt. % HTP for an assumed inlet temperature of 20 °C by means of a black dashed line.
The average temperatures fluctuate between 680 and 705 °C. Note that in most cases the average temperature is higher than the adiabatic decomposition temperature. The HTP is stored in a fridge and gradually warming up to room temperature during tests. In most cases the HTP temperature is below 20 °C when put in the tank. During operation the temperature of the structure, including the part upstream of the catalyst, increases. This causes the temperature of the HTP prior to injection to increase as well. It is believed that the temperature at which the HTP enters the decomposition chamber is in reality higher than the assumed temperature of about 20 °C.

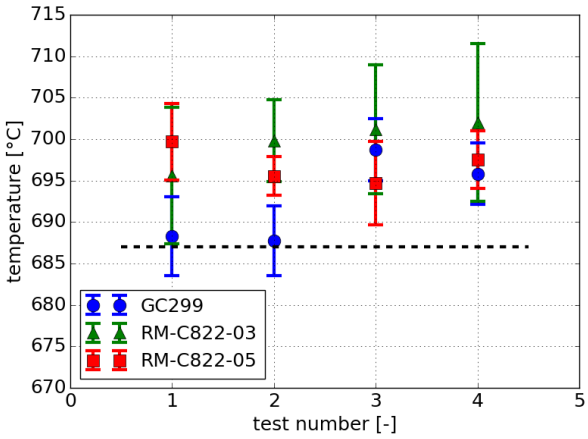

Figure 8: Steady state temperature for slurry C822

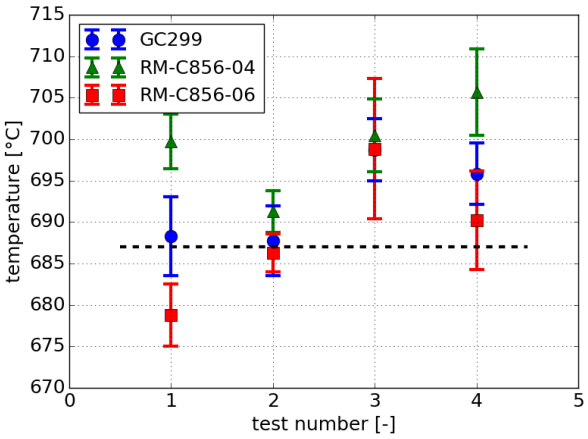

Figure 9: Steady state temperature for slurry C856

The transient performance is shown in Figure 10 through Figure 13. The τ_T-values were determined for different temperatures for monoliths produced from slurry C822 and C856 and are shown in Figure 10 and Figure 11, respectively. The τ_P-values for slurry C822 and C856 are shown in Figure 12 and Figure 13, respectively. Note that the vertical axes have different time scales. In neither case a distinction is made in the order in which the results were obtained.
Figure 10 shows that two out of four runs with monoliths from slurry C822 resulted in very large transient times for temperature. Only in one case, i.e. for slurry C856, the pressure transient time showed a large deviation, see Figure 13. A smaller deviation seems to be present in one of the pressure transient results for slurry C822, see Figure 12. In none of the cases the cause could be determined; no change in operational procedure had occurred.

DOI: 10.13009/EUCASS2017-349

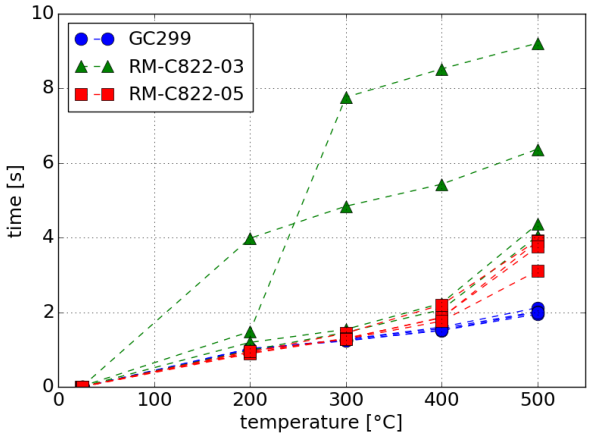

Figure 10: Transient temperature results for slurry C822

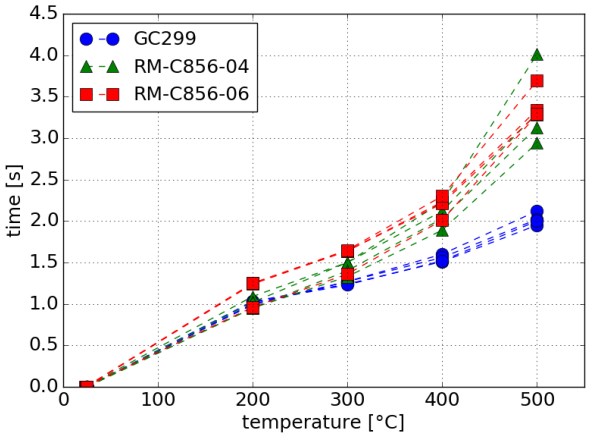

Figure 11: Transient temperature results for slurry C856

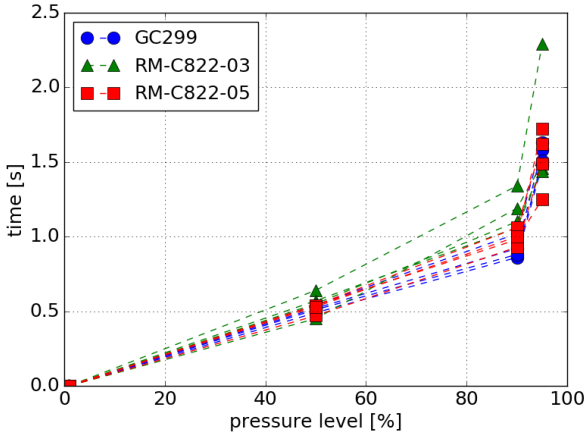

Figure 12: Transient pressure results for slurry C822

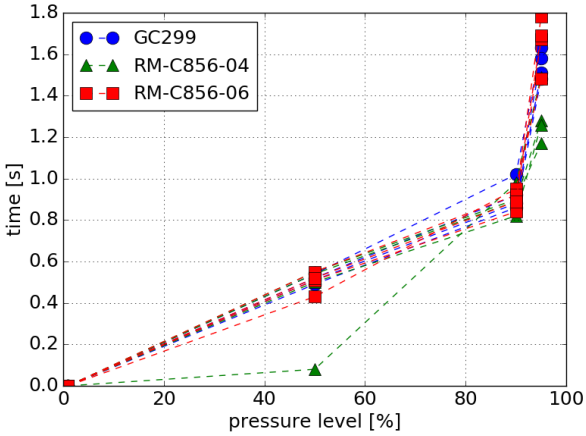

Figure 13: Transient pressure results for slurry C856

6. Discussion

As is shown in Figure 8 and Figure 9, between the tests with one and the same catalyst some variations in average temperature as well as in spread are present. These variations seem to be irregular, i.e. not monotonically in-or decreasing, and cannot be explained by initial aging effects of the catalyst or by the variation in catalyst mass or amount of active phase. The reason for this variation is currently unknown.

The variation in results between the different catalysts is of the same order as the variation between different tests with a single catalyst. In most cases the temperature range is overlapping. Note that in the steady state plots, the temperature measurement uncertainty is not taken into account. The $2\,\sigma$ uncertainty at temperatures of about 700 °C is approximately 4 °C. Taking this into account as well would result in temperature measurements which are overlapping each other. From this it is concluded that there is no difference in steady state temperature between extruded or printed monoliths or between any of the two slurries.

As far as the transient pressure performance is concerned, there seems to be no difference between either of the catalyst, apart from two runs as was already indicated in the previous section. This means that the reactivity of the catalysts is very similar. As can be seen in Table 1, the relative amount of washcoat layer is almost the same for each catalyst. The variation in amount of active phase does not seem to have any influence.

A clear influence on the transient temperature performance is present as is shown in Figure 10 and Figure 11. Catalyst RM-C822-05 seems to perform a little bit better for all temperature levels, despite the slightly higher catalyst mass. The larger mass seems to be offset by the higher amount of active phase present. No distinction in results is noticeable between RM-C856-04 and RM-C856-06. For these catalysts, the mass and amount of washcoat are very similar. Comparing slurry C822 with C856 in Figure 8 and Figure 9, not taking into account the two runs of RM-C822-03 showing outliers, does not reveal any significant difference between the two catalysts.

DOI: 10.13009/EUCASS2017-349

To quantify the effect of catalyst mass, a simplified thermal transient analysis was carried out. For this purpose the heat transfer from the fluid to the channel walls is modelled as

$$A\,h\,(T - T_\infty) = -\rho\,V\,c\,\frac{dT}{dt} \tag{4}$$

Here A is the surface area across which the heat transfer takes place, h the heat transfer coefficient, T the temperature of the wall, T_∞ the temperature of the fluid away from the wall, ρ, V , and c the density, volume and heat capacity of the solid and t the time. As the channel walls are relatively thin, between 0.3 and 0.5 mm, it is assumed that the temperature across the channel walls is uniform, i.e. the Biot number is assumed to be small. Now (4) can be written in terms of a non-dimensional temperature difference

$$\frac{d}{dt}\left(\frac{T-T_\infty}{T_0-T_\infty}\right) + \frac{h\,A}{\rho\,V\,c}\left(\frac{T-T_\infty}{T_0-T_\infty}\right) = 0 \tag{5}$$

Here T_0 is the initial temperature.
The general solution of this differential equation is given by

$$\frac{T-T_\infty}{T_0-T_\infty} = a \cdot \exp\left(-\frac{h\,A\,t}{\rho\,V\,c}\right) \tag{6}$$

where a is a constant of integration dependent on the initial conditions. For the catalysts under investigation, the initial conditions are assumed to be the same and consequently a is the same as well.
For a first approximation, it is further assumed that the heat transfer coefficient, density and heat capacity are the same for all catalysts. If now a certain non-dimensional temperature level is considered then the time for the catalyst to reach this temperature level is dependent on the factor A/V. This ratio was established for catalyst GC299, RM-C822-05 and RM-C856-04 and is listed in Table 2. In this table D and L are the diameter and length of the catalyst, respectively, A_{sol} the solid surface area of the cross section and P the sum of the perimeters of all channels. Note that, here the area is the surface area of the channel walls and the volume the volume of the solid. As they are both taken w.r.t. the same catalyst, this ratio can be calculated by dividing the perimeter P by the solid surface area of the cross section A_{sol}. Given the A/V-ratios in Table 2 and equation (6), to achieve the same temperature difference, catalyst RM-C822-05 would take 2.1 times longer and catalyst RM-C856-04 would take 1.7 times longer, i.e. $(A/V)_{GC299}/(A/V)_{RM}$.

Table 2: Catalyst dimensions

catalyst name	**mass [mg]**	***D* [mm]**	***L* [mm]**	A_{sol} **[mm^2]**	***P* [mm]**	***A/V* [mm^{-1}]**	**mass ratio**	V_{sol} **ratio**	**density [g cm^{-3}]**
GC299	846.3	11.78	10.08	49.2	387.3	7.9	1	1	1.71
RM-C822-05	1709.4	11.86	10.54	76.0	281.7	3.7	2.0	1.6	2.13
RM-C856-04	1442.9	12.12	10.74	72.4	335.9	4.6	1.7	1.6	1.86

Figure 14 shows the τ_T-values for catalysts RM-C822-05 and RM-C856-04 as ratio of the average τ_T-values of catalyst GC299. Catalyst RM-C856-04 requires on average less time to reach 200 °C than catalyst RM-C822-04, even less than GC299, but more time to reach 500 °C than the other two catalysts. As is clear from this figure, the ratio is not a constant value, as would be expected from the theory described above, but increases with temperature. This suggests that the influence of the thermal mass of the catalyst on the performance becomes important only for higher temperatures. Furthermore, Figure 14 seems to show an exponential relationship between the temperature and the time relative to catalyst GC299. This suggests that the original assumption that the temperature across the solid wall is constant, is not valid between the initial temperature rise and reaching steady state temperature. For the current catalysts in the above described configuration this is between 1 and 2 s from the opening of the FCV. However, at 500 °C the relative time w.r.t. catalyst GC299 shown in Figure 14 roughly corresponds to the relative A/V-ratio, i.e. $(A/V)_{GC299}/(A/V)_{RM}$, as was predicted above. In other words, if the transient temperature performance should be maximised, an important parameter to maximise during the design of the internal geometry is the A/V-ratio.
Columns 8 and 9 in Table 2 show the mass of the catalyst relative to the one of GC299 and the volume of the solid phase relative to the volume of the solid phase of GC299, respectively. The volume of the solid phase was determined by multiplying the cross sectional area of the solid phase, i.e. column 5, with the length of the catalyst. Comparison of columns 8 and 9 shows that the mass ratio is very different from the volume ratio for catalyst RM-C822-05 and close but not quite the same for catalyst RM-C856-04. As the material for all three catalysts is the same, from this result it is concluded that the porosity of the printed support structure is different from, i.e. less than, the porosity of the extruded

DOI: 10.13009/EUCASS2017-349

monolith. Furthermore, slurry C822 results in denser structures than slurry C856. The calculated density for each structure is shown in the last column of Table 2.
It would be natural to consider the surface area to density ratio, i.e. A/ρ, the parameter to be optimised as this directly relates the mass of the structure to the area over which the heat transfer takes place. Here, A is determined in the same way as described above, i.e. the perimeter P multiplied by the length of the catalyst L. The values for the relative surface area to density ratio, i.e. $(A/\rho)_{GC299}/(A/\rho)_{RM}$ for RM-C822-05 and RM-C856-04 are 1.64 and 1.18, respectively. Although this gives the same relative order as for the relative A/V-ratio, the actual values do not correspond to the results shown in Figure 14. For this reason the A/V-ratio is preferred to the A/ρ-ratio as the parameter to be optimised.

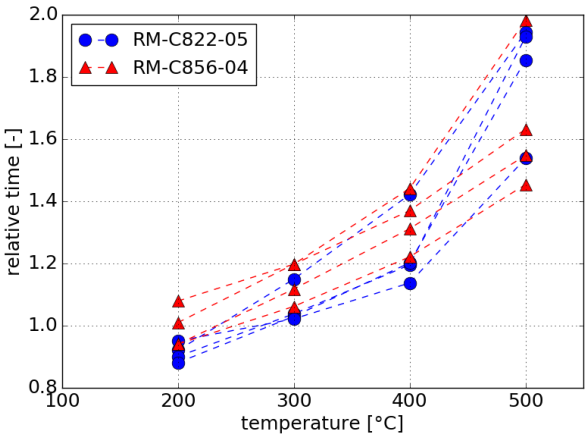

Figure 14: τ_T-values relative to GC299

7. Conclusion

With the recently developed technology for printing ceramic structures, new possibilities open up for optimising monolithic catalysts. Complex 3D internal geometries make it possible to increase the effectiveness of the catalyst while keeping the pressure drop within limits. However, the design cannot be arbitrarily complex. Circular channels with a diameter of 1 mm of less show a deformation of the cross sectional area when the channel has a pitch larger than 0, i.e. for non-straight channels. For circular cross-sectional channels with a diameter of 1.25 mm and larger, this influence becomes noticeable above a pitch of about 2. For channels with a triangular cross section and with a channel density of 600 cpsi, the pitch becomes noticeable from 2.5 onwards.
Decomposition tests revealed that there is no difference in steady state temperature performance when comparing catalysts with a printed support structure with catalysts with an extruded support structure. In both cases the measured temperature is above the adiabatic decomposition temperature of 87.5 wt. % HTP. This is attributed to a preheating effect: prior to injection the hydrogen peroxide is heated up to well above the assumed initial temperature of 20 °C.
The transient pressure performance is not affected either by the manufacturing process of the monoliths. An effect is visible though for the transient temperature response. It was determined that an increase in the temperature transient time is proportional to the A/V-ratio of the printed catalysts compared to the extruded catalyst. This is noticeable during the second half of the transient phase.
It was also revealed that the porosity of the different catalysts is different. In general, the porosity is larger for the printed structures. The type of slurry also influences the porosity. A relatively large difference in bulk density was found between slurry C822 and slurry C856 with a density of 2.13 and 1.86 g·cm^{-3}, respectively. The test results show that a less dense structure, i.e. a larger porosity, improves the transient temperature response. It was also found that the A/V-ratio is a better indicator for the response time than the A/ρ-ratio.
Finally, it was shown that during the second half of the transient phase the assumption of a uniform temperature across the wall is not valid. As a consequence, the first half of the transient phase is not affected by thermal mass of the system, but the second half is. This is important to take into account when modelling the thermal response of the catalyst during the transient phase.
It should be noted that the difference in performance between extruded and printed monoliths is caused by a difference in thermal mass and porosity of the support structure. The larger solid volume of the printed monoliths in this study is not a limitation of the manufacturing process, but the result of the current manufacturing process settings. By optimising the printing process thinner structures can be printed. From experience it is known that the wall thickness can be reduced to less than 0.2 mm. In that case the solid volume of the printed monoliths will be very similar to the extruded monoliths.

DOI: 10.13009/EUCASS2017-349

Acknowledgement

This project has received funding from the European Union's Horizon 2020 research and innovation programme under grant agreement No. 640376.

References

[1] A. J. Musker *et al.*, 'Realistic Testing of PX1 Catalyst Using Near-Anhydrous Hydrogen Peroxide', presented at the Space Propulsion Conference 2016, Rome, Italy, 2016.
[2] D. Zube, S. Christofferson, E. Wucherer, and B. Reed, 'Evaluation of HAN-Based Propellant Blends', presented at the 39th AIAA/ASME/SAE/ASEE Joint Propulsion Conference and Exhibit, Huntsville, Alabama, USA, 2003.
[3] D. Krejci *et al.*, 'Assessment of Catalysts for Hydrogen-Peroxide-Based Thrusters in a Flow Reactor', *J. Propuls. Power*, vol. 29, no. 2, pp. 321–330, Mar. 2013.
[4] M. J. Palmer, A. J. Musker, G. T. Roberts, and C. Ponce-de-Leon, 'Manufacture , Assessment and Down-Selection of Catalysts for the Decomposition of Hydrogen Peroxide', in *Proceedings of the 4th European Conference for Aerospace Sciences (EUCASS)*, St. Petersburg, Russia, 2011.
[5] S. Dolci, D. B. Dell'Amico, A. Pasini, L. Torre, G. Pace, and D. Valentini, 'Platinum Catalysts Development for 98% Hydrogen Peroxide Decomposition in Pulsed Monopropellant Thrusters', *J. Propuls. Power*, vol. 31, no. 4, pp. 1204–1216, Jul. 2015.
[6] K. Essa *et al.*, 'Development and Testing of an Additive Manufactured Catalyst Bed for HTP Thruster Applications', presented at the Space Propulsion Conference 2016, Rome, Italy, 2016.
[7] R. A. Spores, 'GPIM AF-M315E Propulsion System', presented at the 51st AIAA/SAE/ASEE Joint Propulsion Conference, Orlando, Florida, USA, 2015.
[8] S. A. Whitmore, D. P. Merkley, M. I. Judson, and S. D. Eilers, 'Development and Testing of a Green Monopropellant Ignition System', 2013.
[9] E. J. Wucherer, T. Cook, M. Stiefel, R. Humphries, and J. Parker, 'Hydrazine Catalyst Production - Sustaining S-405 Technology', presented at the 39th AIAAlASME/SAE/ASEE Joint Propulsion Conference and Exhibit, Huntsville, Alabama, USA, 2003, vol. AIAA 2003-5079.
[10] T. W. Price and D. D. Evans, 'The Status of Monopropellant Hydrazine Technology', Jet Propulsion Laboratory, Pasadena, California, USA, Technical Report TR-32-1227, Feb. 1968.
[11] 'DLR - Institut für Raumfahrtantriebe - Rheform at a glance'. [Online]. Available: http://www.dlr.de/ra/desktopdefault.aspx/tabid-10285/17619_read-42041/. [Accessed: 10-Mar-2017].
[12] M. Schwentenwein and J. Homa, 'Additive Manufacturing of Dense Alumina Ceramics', *Int. J. Appl. Ceram. Technol.*, vol. 12, no. 1, pp. 1–7, Jan. 2015.
[13] R.-J. Koopmans *et al.*, 'Experimental Investigation and Analysis of Catalysts for Hydrogen Peroxide Based Thrusters', presented at the Space Propulsion 2016, Rome, Italy, 2016.
[14] D. Krejci, A. Woschnak, C. Scharlemann, and K. Ponweiser, 'Structural impact of honeycomb catalysts on hydrogen peroxide decomposition for micro propulsion', *Chem. Eng. Res. Des.*, vol. 90, no. 12, pp. 2302–2315, Dec. 2012.
[15] C. Maleix *et al.*, 'Development of catalytic materials for decomposition of ADN-based monopropellants', in *Proceedings of the 7th European Conference for Aerospace Sciences (EUCASS)*, Milan, Italy, 2017.